Design and Performance Analysis of Depletion-Mode InSb Quantum-Well Field-Effect Transistor for Logic Applications

R. Islam[1], M. M. Uddin[2*], M. Mofazzal Hossain[3], M. B. Santos[4], M. A. Matin[1], and Y. Hirayama[5]

[1]*Department of Electrical & Electronic Engineering, Chittagong University of Engineering & Technology (CUET), Chittagong 4349, Bangladesh*

[2]*Department of Physics, Chittagong University of Engineering & Technology (CUET), Chittagong 4349, Bangladesh.*

[3]*Department of Electronics and Communications Engineering, East West University, Plot No-A/2, Jahurul Islam City, Aftabnagar Main Road, Dhaka 1219*

[4]*Homer L. Dodge Department of Physics and Astronomy, University of Oklahoma, 440 West Brooks, Norman, Oklahoma 73019-2061, USA*

[5]*Department of Physics, Tohoku University, Sendai, Miyagi 980-8578, Japan*

[*]*E-mail: mohi@cuet.ac.bd*

Abstract:

The design of a 1 μm gate length depletion-mode InSb quantum-well field-effect transistor (QWFET) with a 10 nm-thick Al_2O_3 gate dielectric has been optimized using a quantum corrected self-consistent Schrödinger-Poisson (QCSP) and two dimensional drift-diffusion model. The model predicts a very high electron mobility of 4.42 $m^2V^{-1}s^{-1}$ at V_g= 0V, a small pinch off gate voltage (V_p) of -0.25V, a maximum extrinsic transconductance (g_m) of ~ 4.94 S/mm and a drain current density of more than 6.04 A/mm. A short-circuit current-gain cut-off frequency (f_T) of 374 GHz and a maximum oscillation frequency (f_{max}) of 645 GHz are predicted for the device. These characteristics make the device a potential candidate for low power, high-speed logic electronic device applications.

Introduction:

The realization of improved high-performance transistors has become increasingly challenging due to difficult requirements for reduced power dissipation during operation and in stand-by mode, which are necessary to meet Moore's Law by scaling down Si-based complementary metal-oxide-semiconductor (CMOS) devices [1,2]. Moreover, increasing operating frequency and higher integration density make the power constraint issue even more challenging. Therefore, researchers have devoted much effort to develop high-performance transistors that use a low supply voltage.

Recently, many studies have focused on high-mobility channel materials such as carbon nanotubes [3], silicon nanowires [4], graphene [5], Ge [6] and III-V semiconductors [7-11]. These materials have a much higher electron mobility than in silicon. Therefore, they are potential candidates for high-speed transistors with very low supply voltage. Extensive research has been carried out with many of the III-V semiconductors (GaAs, InAs, InGaAs, GaN, GaSb, etc.) as channel material [12-17]. However, there have been fewer efforts to fabricate transistors made from InSb because of problems in the fabrication process. It is difficult to form a good interface between the top InSb (or AlInSb) layer and a subsequently deposited insulator due to a rough initial surface. There are a few reports on the formation of a high-quality gate dielectric on InSb/AlInSb and the fabrication of high-performance InSb quantum well field effect transistors (QWFETs), although the optimum layer structure for the highest performance has not been identified yet [7-10]. In this report, we determine the optimized InSb QWFET layer structure and predict its performance using a quantum corrected self-consistent Schrödinger-Poisson (QCSP) and two dimensional drift-diffusion model. It is noteworthy that our optimized InSb QWFET is expected to exhibit a very high electron mobility (μ), a low pinch off gate

voltage (V_p) and the highest cut-off frequency (f_T) ever reported in the InSb system. Identification of an optimized InSb QWFET structure is an important step toward realizing InSb-based high-speed and low power logic electronics applications.

Simulation Details:

The electronic states in confined semiconductor structures such as a quantum well are controlled by size quantization where so called energy subbands are formed. The electronic subbands of the conduction band and the corresponding envelope functions can be determined by solving the Schrödinger equation self-consistently with the Poisson equation [18]. When two or more semiconductors sandwiched together, the Fermi levels align when equilibrium is reached. The bands of an individual layer tend toward their bulk positions, resulting in band bending near the interface. The electric field created by band bending assists in bring the Fermi levels into equilibrium alignment with each other. The energy eigenvalues and wave functions are calculated by incorporating the potential due to the carrier density into the Schrödinger equation.

$$-\frac{\hbar^2}{2m^*}\frac{d^2}{dx^2}\psi(x)+V(x)\psi(x)=E\psi(x) \qquad (1)$$

where m* is the effective mass, $\hbar$ is the Planck constant h divided by 2π, $V(x)$ is the potential, $\psi(x)$ is the wave function and E is the energy.

The electrostatic potential $\phi(x)$ is then calculated by Poisson's equation;

$$\nabla.[\epsilon_0\epsilon_r(x)\nabla\phi(x)] = -\rho(x) \qquad (2)$$

where ρ is the charge per unit volume, ε_0 is the vacuum permittivity and the tensor ε_r is the material dependent dielectric constant at position x. The charge density distribution $\rho(x)$ within a semiconductor device is represented by

$$\rho(x) = e\left[-n(x) + p(x) + N_D^+(x) - N_A^-(x) + \rho_{fix}(x)\right] \tag{3}$$

where e is the positive elementary charge, n and p are the electron and hole densities, N_D^+ and N_A^- are the ionized donor and acceptor concentrations, respectively, and ρ_{fix} is the fixed or volume charge densities which arise from piezo or pyroelectric charges. In a quantum well of arbitrary potential energy profile, the potential energy $V(x)$ in Equation (1) is related to the electrostatic potential ϕ:

$$V(x) = -q\phi(x) + \Delta E_c(x) \tag{4}$$

where $\Delta E_c(x)$ is the pseudopotential energy due to the band offset at the heterointerfaces.

Equations (1) and (2) have been iteratively used to obtain self-consistent solutions of the Schrödinger and Poisson equations. The electron density distribution function $n(x) = \sum_{k=1}^{m} \psi_k^*(x)\psi_k(x)n_k$, (where n_k is electron occupation for each state and m is the number of subbands) has been calculated using a trial potential $V(x)$, the wave functions $\psi(x)$, and their corresponding eigenenergies, E_k. The electron density in each state is described by $n_k = \frac{m^*}{\pi\hbar^2}\int_{E_k}^{\infty} \frac{1}{1+e^{(E-E_F)/kT}}dE$, (where K is the Boltzmann constant and T is the measuring temperature). The electrostatic potential $\phi(x)$ in equation (4) is then calculated by using the computed $n(x)$ and donor concentration $N_D(x)$. The new potential energy $V(x)$ in equation (4) has

been obtained using the computed $\phi(x)$. In this way, there is a closed loop for solving the Schrödinger equation, calculating the potential due to the resulting charge distribution, adding it to the original band-edge potential, solving Schrödinger equation again, and so on until the update is below a certain limit, indicating that convergence has been reached. Thus, the band profile of a QW has been calculated using self-consistent Schrödinger and Poisson solutions.

The temperature dependent band gap E_g can be calculated by $E_g(T) = E_g(T = 0) - \alpha T^2/(T + \beta)$, where the Varshni parameters for InSb are $\alpha = 0.32\ meV/K$ and $\beta = 170\ K$ [19] and for the alloy $Al_xIn_{1-x}Sb$ can be calculated by $E_g(x) = E_g(0) + (2.0\ eV)x$ [20].

The characteristics of charge transport in the QWFET is of fundamental importance for electronic device applications. Charge transport in the device has been calculated using the simplest drift-diffusion model (DDM) by taking zeroth order moments of the Boltzmann Transport Equation (BTE) and adjoining the Poisson equation [21]. The drift diffusion current density expressions for electrons and holes are

$$J_n(x) = q\mu_n n(x)E(x) + qD_n \frac{dn(x)}{dx}$$

$$J_p(x) = q\mu_p p(x)E(x) - qD_p \frac{dp(x)}{dx}$$

where μ_n and μ_p are the electron and hole mobility, D_n and D_p are the electron and hole diffusivity. The first part of the above equations represents the drift current, while the second part represents the diffusion current.

DEVICE STRUCTURE

The effects of parameters for the spacer layer, barrier layers, doping concentration, QW width and dn_s/dV_g on the electron density and mobility of an InSb QWFET have been calculated using QCSP solutions, and can be found elsewhere [22]. Fig. 1 shows the cross-sectional view of an InSb QWFET structure with a 10 nm-thick Al_2O_3 gate insulator, which has been optimized for high electron mobility and a small V_p. The buffer layer of the device consists of a 3μm $Al_{0.1}In_{0.9}Sb$ layer with an $Al_{0.2}In_{0.8}Sb$ interlayer, a 20 nm-thick InSb quantum well as the channel layer, a 45 nm $Al_{0.1}In_{0.9}Sb$ barrier layer with a 25 nm spacer layer and a 2 nm Si δ-doped layer with 1×10^{12} cm^{-2} *n*-type doping density located 25 nm above the QW channel. Indium can be used to define the source, drain and top gate metal. Details of ALD deposition of an Al_2O_3 gate insulator have been presented elsewhere [10,11].

Results and discussion:

The band profile (conduction band minimum, E_c, and valence band maximum, E_v) of the optimized InSb QWFET at different V_g was calculated using the QCSP model, and is shown in Fig. 2, where E_F is at 0 eV and E_c at zero depth is equal to the Schottky barrier height (ϕ_B). The fitting parameter ϕ_B is determined by properties of the semiconductor surface and interface states between the gate insulator Al_2O_3 and top $Al_{0.1}In_{0.9}Sb$ layer. The value of ϕ_B is equal to the energy difference between E_c at zero depth and E_F under thermal equilibrium conditions. The donor density of the δ-doping layer (1×10^{12} cm^{-2}) is set so that the E_c (at V_g=0V) is located above the E_F thus precluding the formation of a parallel conduction channel. The QW is the only conduction channel. It is notable that the relatively wide band gap ~ 0.42 eV [20] of $Al_{0.1}In_{0.9}Sb$ positions the E_v far away from the E_F at zero depth, which prevents hole accumulation at the surface. The CBM moves to higher energy at negative V_g, resulting in a decrease of n_s in the QW

(Fig. 2). At V_g = -0.25V, E_c is lifted above the E_F which confirms the complete depletion of the n_s in the QW and E_v at the surface is just below E_F as shown in Fig. 2. The confined 2DEG in the InSb QW is completely depleted with a very small V_g= -0.25V [22]. This very small pinch–off voltage, V_p, has been achieved due to very low interface trap density (D_{it}) [The Gauss law gives $Q_{it} = \varepsilon_0\varepsilon_{ox}E_{ox} - \varepsilon_0\varepsilon_{sc}E_{sc}$ (electric field $E_{ox}= V_{ox}/d_{ox}$ with Al_2O_3 thickness d_{ox} = 10 nm, electric field E_{sc} at the semiconductor surface obtained from the QCSP simulation). The D_{it} has been determined using the equation $dQ_{it}/d(E_F\text{-}E_v) = -eD_{it}$,[23]] and consequently a very large gate controllability ratio of dn_s/dV_g = ~ $5.2 \times 10^{15} m^{-2}V^{-1}$ (estimated in the range of $-0.2V \leq V_g \leq 0V$) is predicted as discussed in ref. 22.

The gate voltage (V_g) dependence of total mobility ($\mu = \frac{e\langle\tau\rangle}{m^*(E)}$) of the InSb QWFET has been calculated using QCSP model. Total mobility (μ) is estimated according to the Matthiessen's rule, $\frac{1}{\mu_{total}} = \frac{1}{\mu_{imp}} + \frac{1}{\mu_{bg}} + \frac{1}{\mu_{acoustic}} + \frac{1}{\mu_{polar}}$, where μ_{imp}, μ_{bg}, $\mu_{acoustic}$, and μ_{polar} are the mobility due to the ionized impurity, ionized background impurity, acoustic phonon impurity and polar optic phonon scattering, respectively. Details of various scattering process are described elsewhere [22]. The calculated V_g dependent electron mobility (μ) is shown in Fig. 3. A very high electron mobility 4.42 $m^2V^{-1}s^{-1}$ at V_g= 0V is achieved which is at least ~180 times greater than that of Si NMOS [7].

Figure 4 shows the well behaved I-V characteristics of the optimized InSb QWFET calculated as a function of gate bias with a 10 nm-thick Al_2O_3 gate dielectric. The plot shows a clear pinch off at a gate voltage of -0.35V which is very close to V_p obtained from the band profile (Fig. 2) and the n_s-V_g plot (in ref. 22). The V_g is varied from 0 to -0.35 V with a 0.05 V step. The drain current does not show noticeable hysteresis during forward and reverse gate voltage sweeping

directions. It indicates that no significant mobile bulk oxide charge is present in the gate insulator thereby the density of slow interface traps is low. The maximum drain current density I_{ds}/W_g at V_g=0V is approximately 40 μA/μm.

The gate bias dependent drain current in the saturation region of the InSb QWFET device is shown in Fig. 5 (black squares). The device shows the quasilinear relation between I_{ds} vs V_{gs} in the wide bias range. The transconductance represents the ability of the FET to amplify the signal and is denoted by the output/input ratio, $g_m = dI_d/dV_{gs}$. The slope of the drain current (I_{ds}) yields the extrinsic g_m of the 1 μm gate length device and is shown in Fig. 5 (blue squares). The maximum extrinsic g_m is found to be ~ 4.94 S/mm. The very high g_m of the device indicates the high speed capability of the device. Since the mobility of the device is very high, the g_m is also high (g_m = V μ W c_i /L, where V represents the drain-source voltage, μ is the mobility, W is the gate width, c_i is the gate capacitance and L is the gate length of the device). It is noted that both the quasilinear I_{ds} vs V_{gs} and the wide g_m vs V_{gs} show no significant hysteresis in forward and reverse bias directions. Counting the series resistance of the device R_s ~2.5 Ω mm, the theoretical extrinsic transconductance (g_m) $\{g_{max}=\frac{g_m}{1+R_s g_m}\}$ is 3.7 S/mm which is almost 40% off from the peak g_m value of 5.6 S/mm (Fig. 5).

The cut-off frequency f_T and the maximum frequency of oscillation f_{max} of the device are commonly used to measure high-speed capability. The f_T is defined as the frequency of unity gain, at which the small-signal input gate current is equal to the drain current of the intrinsic FET. From S-parameter measurements, the short-circuit current-gain f_T and the f_{max} are determined by biasing the devices at V_{ds}=0.5V and V_g=0V. Under these conditions, the values of f_T and f_{max} are calculated to be 374 and 645 GHz, respectively. Extrapolating the short-circuit

current gain (H_{21}) and the unilateral power gain (U) curves to unity and the 20 dB/decade slopes are used to determine the values of f_T and f_{max}, respectively as shown in Fig. 6.

Conclusions:

We have demonstrated design and performance analysis of a depletion mode optimized InSb QWFET using a quantum corrected self-consistent Schrödinger-Poisson (QCSP) and two dimensional drift-diffusion model. The device with a 1µm gate length and 100µm gate width shows a very high electron mobility of 4.42 $m^2V^{-1}s^{-1}$ at V_g= 0V and a small pinch off voltage of -0.25V. The device is predicted to have the highest cut-off frequency f_T and maximum frequency of oscillation f_{max} ever reported in the InSb system. These results indicate that the optimized InSb QWFET has a strong potential in low power and high-speed nanoelectronics applications.

Acknowledgements: The authors are grateful to Dr. S. Birner for fruitful discussions.

References:

1. Jesús A. del Alamo, *Nature*, **479**, 317 (2011).
2. R. Chau, B. Doyle, S. Datta, J. Kavalieros and K. Zhang, *Nature Materials*, **6**, 810 (2007)
3. Ray H. Baughman, Anvar A. Zakhidov, Walt A. de Heer, *Science*, **297**, 787 (2002).
4. Y. Cui, Z. Zhong, D. Wang, W. U. Wang and C.M. Lieber, *Nano Lett.*, **3**, 149 (2003).
5. Frank Schwierz, *Nature Nanotechnology*, **5**, 487 (2010).
6. J. Xiang, W. Lu, Y. Hu, Y. Wu, H. Yan and C.M. Lieber, *Nature*, **441**, 489 (2006).
7. S. Datta, T. Ashley, J. Brask, L. Buckle, M. Doczy, M. Emeny, D. Hayes, K. Hilton, R. Jefferies, T. Martin, T. J. Phillips, D. Wallis, P. Wilding, and R. Chau, Te*ch. Dig. - Int. Electron Devices Meet.*, 763 (2005).
8. R. Chau, S. Datta, M. Doczy, B. Doyle, B. Jin, J. Kavalieros, A. Majumdar, M. Metz, and M. Radosavljevic, *IEEE Trans. Nanotech.*, **4**, 153 (2005).

9. T. Ashley, L. Buckle, S. Datta, M. T. Emeny, D. G. Hayes, K. P. Hilton, R. Jefferies, T. Martin, T. J. Philips, D. J. Wallis, P. J. Wilding, and R. Chau, *Electron. Lett.*, **43**, 777 (2007).
10. M. M. Uddin, H. W. Liu, K. F. Yang, K. Nagase, K. Sekine, C. K. Gaspe, T. D. Mishima, M. B. Santos, and Y. Hirayama, *Appl. Phys. Lett.*, **103**, 123502 (2013).
11. M. M. Uddin, H. W. Liu, K. F. Yang, K. Nagase, T. D. Mishima, M. B. Santos, and Y. Hirayama, *Appl. Phys. Lett.*, **101**, 233503 (2012).
12. P. D. Ye,G. D. Wilk, B. Yang, J. Kwo, S. N. G. Chu, S. Nakahara, H.-J. L. Gossmann, J. P. Mannaerts, M. Hong, K. K. Ng, and J. Bude, *Appl. Phys. Lett.*, **83**, 180 (2003)
13. Y. Xuan, T. Shen, M. Xu, Y.Q. Wu, and P.D. Ye, Te*ch. Dig. - Int. Electron Devices Meet.*, 371 (2008).
14. P. D. Ye,B. Yang, K. K. Ng, and J. Bude, G. D. Wilk, S. Halder and J. C. M. Hwang, *Appl. Phys. Lett.*, **86**, 063501 (2005).
15. T.-W Kim, R.J.W. Hill, C.D. Young, D. Veksler, L. Morassi, S. Oktybrshky, J. Oh, C.Y. Kang, D. Kim, J. A. del Alamo, C. Hobbs, P. D. Kirsch, R. Jammy, In *Symposium on VLSI Technology(VLSIT)*, (2012).
16. N. Li, E. S. Harmon, J. Hyland, D. B. Salzman, T. P. Ma, Yi Xuan, and P. D. Ye, *Appl. Phys. Lett.* **92**, 143507 (2008).
17. M. Xu, R. Wang, P. D. Ye, *IEEE Electron Device Letters*, **32** (7), 883 (2011).
18. I-H Tan, G. L. Snider, D. L. Chang and E. L. Hu, *J. Appl. Phys.*, **68**, 4071 (1990).
19. I. Vurgaftman, J. R. Meyer, and L. R. Ram-Mohan, *J. Appl. Phys.*, **89**, 5815 (2001).
20. N. Dai, F. Brown, P. Barsic, G. A. Khodaparast, R. E. Doezema, M. B. Johnson, S. J. Chung, K. J. Goldmmer, and M. B. Santos, *Appl. Phys. Lett.* , **73**, 1101 (1998).
21. Ansgar Jüngel. *Transport equations for semiconductors*. Vol. 773, P. 99, Springer, (2009).
22. R. Islam, M. M. Uddin, M. A. Matin, *ECS Transactions*, **69**(5), 3 (2015).
23. S. M. Sze and K. K. Ng, *Physics of Semiconductor Devices*, 3rd ed. (John Wiley & Sons, New York, 2007).

Figure captions

Figure 1. Cross sectional view of optimized InSb QWFET layer structure with L_G = 1μm and W_g=100 μm. The Si δ-doping layer is indicated by a dashed line.

Figure 2. Band profile of the InSb QWFET at different gate bias (V_g) is calculated by self-consistent Schrödinger-Poisson (SP) model. The depth is along the growth direction and the corresponding layer structures are indicated at the bottom axis. E_c and E_v represent the conduction-band minimum and the valence-band maximum energies, respectively and the Fermi energy E_F is set to 0 eV. E_1 shows the first eigen energy state for different V_g. The vertical arrows denote the Si δ-doped regions in the AlInSb layers.

Figure 3. The calculated gate bias (V_g) dependence of electron mobility (μ) in the InSb QWFET at 300 K.

Figure 4. Calculated drain current vs. drain bias as a function of gate bias of InSb Quantum Well FET with a 10 nm Al_2O_3 gate dielectric.

Figure 5. Calculated gate bias dependent drain current (black squares) and the extrinsic transconductance g_m (blue squares) of the InSb QWFET device. The device is in the saturation region, biased at V_{ds} = 1V.

Figure 6. Calculated current (H_{21}) and unilateral power (U) gain as a function of frequency for an InSb QWFET device with a 1μm gate length (L_g) and 100 μm gate width (W_g). Inset: magnified view of the unity portion of the curves.

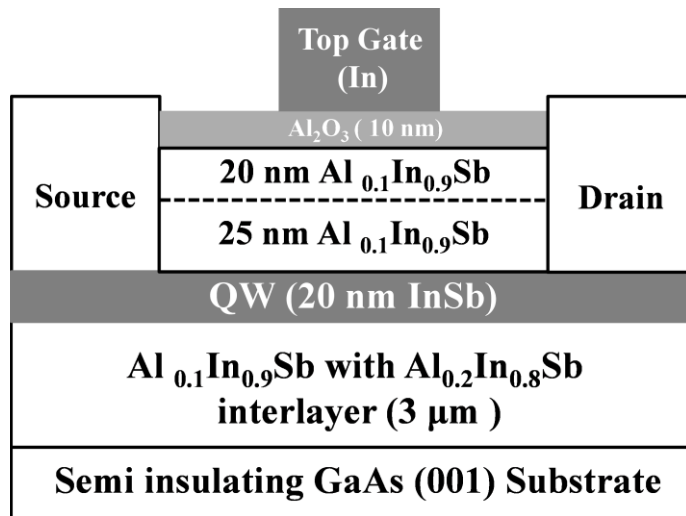

Figure 1.

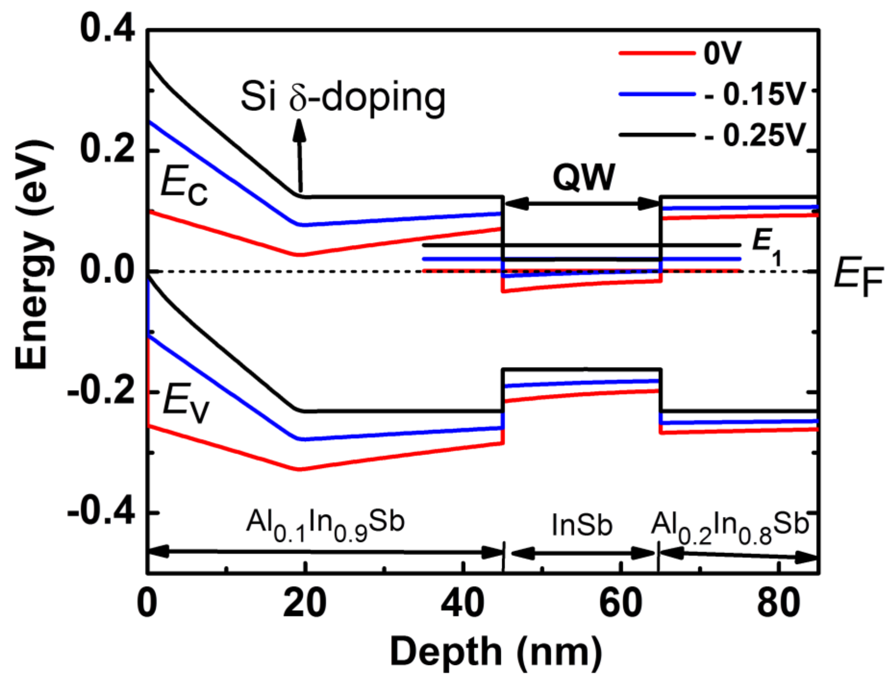

Figure 2.

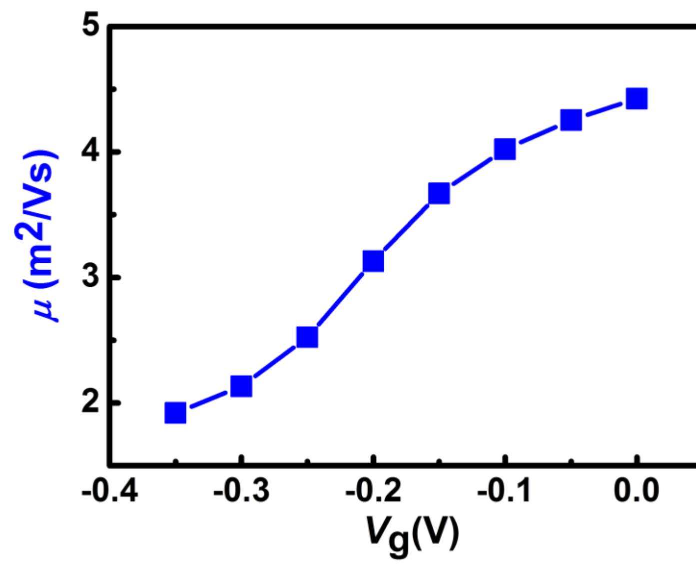

Figure 3.

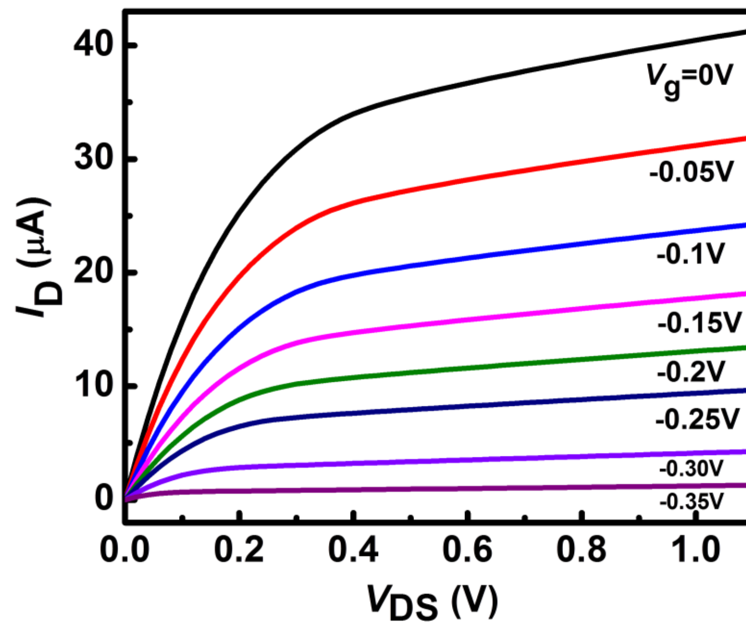

Figure 4.

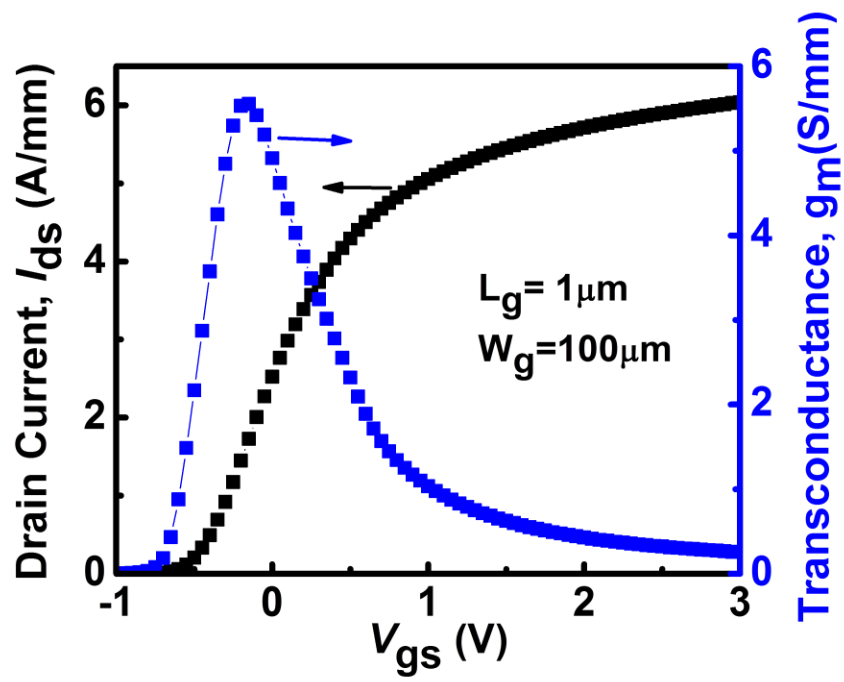

Figure 5.

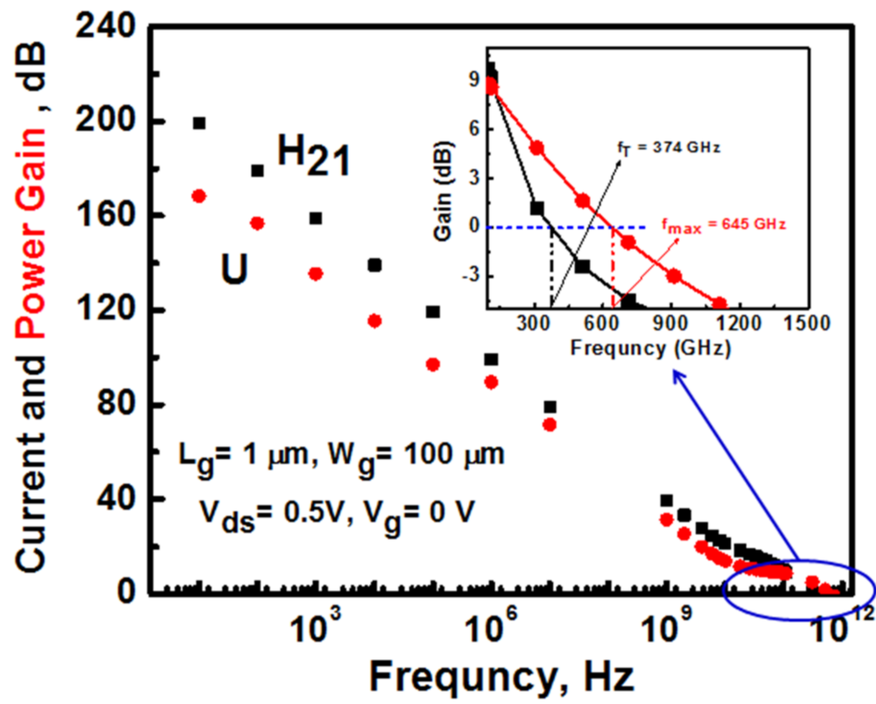

Figure 6.